JOURNAL OF MATERIALS SCIENCE **38** (2003) 803–815

Near-surface deformation under scratches in polypropylene blends

Part I *Microscopic characterization of deformation*

HOUXIANG TANG*, D. C. MARTIN‡
Department of Materials Science and Engineering, University of Michigan, Ann Arbor, MI 48109-2136, USA
E-mail: milty@umich.edu

A microstructural characterization approach has been developed to study the mechanisms of near-surface deformation under surface scratches in injection-molded polypropylene blends with over 20% rubber modifier (thermoplastic polyolefin or TPO). The near-surface microstructure of the material before and after scratching was characterized with different techniques such as transmission electron microscopy (TEM), scanning electron microscopy (SEM), optical microscopy and X-ray diffraction. It was observed that the TPO material plastically deformed by forming shear band structure under surface scratches. Materials inside shear band dilated and the extent of dilation could be measured from the characteristic angles between the shearband boundary and rubber particles. At a higher applied normal load (>200 g for the test in this study), evidence for surface fracture was observed. At even higher loads (>400 g), significant amounts of sub-surface voiding were observed, due to the delamination between the rubber phases and the polypropylene matrix. The observation of both the dilation of materials inside shearbands and the subsurface voiding at high normal loads advanced the understanding of scratching whitening mechanism in this kind of important materials. It was observed that the talc additives had no obvious influence on shear band nucleation and propagation. Results obtained in this study suggest that a strong interfacial adhesion between rubber phase and PP matrix is crucial to improving the scratching resistance of rubber modified polypropylene blends.

1. Introduction

Polypropylene blends with over 20% rubber phase (thermoplastic polyolefins or TPOs) have been widely used in the automotive industry both as interior and exterior parts. Unpainted TPO materials are generally very susceptible to scratch damage, which degrades both the aesthetic value and the durability of components.

The scratching of a single asperity over the surface of interest has been a widely adopted method in studying near-surface mechanical properties of materials. In the study of the tribology of rubber materials, Shallamach observed that regular folds of material, now known as "Shallamach waves," formed under a blunt rigid asperity when it moved over a rubber surface [1]. It was believed that the stick-slip motion between the tip and the rubber surface gave rise to the Shallamach waves. By monitoring the force acting at the interface and optical study of the wave structure, the frictional energy could be correlated with the scratch testing conditions and the mechanical properties of the material [2, 3]. Further studies of the periodic patterns established a relationship between features of the pattern geometry (i.e. width and wavelength), material properties (i.e. friction coefficient and Young's modulus) and testing conditions (i.e. scratch speed, tip attacking angle) [4–8]. However, in these studies, very little attention was paid to the materials left behind the scratch and damage caused by the friction.

In the last two decades, considerable effort has been made to correlate scratching behavior with structures and properties in different kinds of polymers and polymer composites [9–12]. Briscoe and coworkers have studied different factors that influence the deformation modes of polymeric materials under scratches [13–15]. It has been summarized that with increasing scratching severity, the material underwent different characteristic deformation modes: elastic, ironing, ductile plowing, ductile machining plus cracking, until brittle machining. Testing conditions that influence the deformation modes include the shape of the scratch tip, normal load, sliding velocity, interfacial lubrication,

* *Present Address:* The Dow Chemical Company, Analytical Laboratory, Building 1897E, Midland, MI 48667, USA.
‡ Author to whom all correspondence should be addressed.

and testing temperature. Different surface characterization techniques have been used to study surface deformation, such as scanning electron microscopy (SEM) and laser profilometry. By monitoring the force at different temperatures and scratching speeds, efforts have been made to correlate the deformation with the mechanical properties of the material, such as elasticity, plasticity and viscoplasticity [16–18].

One of the parameters often used to assess scratch damage is the wear coefficient, which is defined as:

$$\text{Wear\_Coefficient} = \frac{\text{Wear\_Volume}}{\text{Normal\_Load} \times \text{Sliding\_Length}}$$

Czichos *et al*. [11] studied the influence of different parameters on the wear coefficients of different polymers and polymer composites. In the study of nano-tribology of polymeric materials, atomic force microscopy (AFM) is often used to measure the topography of scratches and RMS roughness as a parameter of scratch severity [19–21]. Blackman and coworkers studied the influence of applied normal load on the wear rate of coating materials with an instrumented scratch tester coupled with AFM [22, 23]. An excess of volume in the pile up was observed that could not be explained by the volume removed by the indenter. The authors ascribed the excess of volume to the subsurface brittle cracking. However, no direct imaging of cracking was presented.

In recent years, several qualitative and quantitative methods have been developed to assess scratch visibility in polymeric materials. Kody and Martin [24] developed a method using reflected polarized light microscopy to quantitatively characterize the light scattered from scratches in polypropylene blends. Chu *et al*. [25–27] characterized light scattering from scratches in different mineral filled polypropylene materials. Besides quantitative measurement of light scattering from scratches, qualitative surveys have been adopted to investigate the influence of different material and testing factors on scratch visibility [23, 28]. Light scattering from scratches is generally ascribed to structural inhomogeneity caused by deformation under the scratch, such as shear deformation zones, crazes, and brittle cracks. At low applied normal loads, brittle materials give rise to smaller plastic zones under scratches resulting in less light scattering compared with scratches in ductile materials. However brittle materials generally reach failure thresholds at lower loads and the light scattering increases dramatically when brittle cracking happens [28].

It is generally believed that the relatively low elastic modulus and yield strength of the PP matrix contribute to the susceptibility of TPO materials to surface damage. Xiang *et al*. [29] studied the scratching behavior of different polymers, using optical microscopy and SEM to characterize the subsurface damage. An attempt to correlate simple material properties (i.e. Young's modulus, yield strength) with scratching behavior was made. Even though the authors mentioned that it was necessary to take into account different material parameters to properly explain the scratching behavior, they did not provide any effort in this direction. In studies utilizing both subjective visual assessments and quantitative reflectivity measurements, several groups found that it was not the total area of the scratch, but the relative change in the grey level of the scratched areas that controlled the scratch visibility [30, 31]. Lau *et al*. reported that the light scattering from a scratch increased with normal load initially and leveled off at high normal load [32].

The design of TPO materials with improved scratch resistance is still an ongoing challenge in industry [33, 34]. TPO has a multi-phase structure composed of PP matrix, rubber particles and mineral additives. Each phase and the interactions between different phases should all influence the near-surface mechanical properties of the material. To understand the characteristics of these multiple structural factors influencing deformation behavior, detailed structural characterization of the deformed material is necessary. Quantitative measurements of the intensity of light scattering and surface topography characterization provide relatively little structural information. Optical microscopy and SEM suffer from poor spatial resolution and the lack of phase differentiation. In our research, we mainly adopted transmission electron microscopy to characterize the near-surface deformation in TPOs under scratches. We believe that the results reported here provide new understanding about this subject.

2. Experimental procedures

2.1. Materials

The TPO materials studied in this research were injection-molded blends of isotactic polypropylene with about 20 wt% ethylene/propylene/diene terpolymers (EPDM) rubber and about 5 wt% talc additive. The side-gated plaques with a dimension of $30 \times 30 \times 0.3$ cm were supplied by DuPont Automotive, and used without further treatment.

2.2. Scratching tests

The scratching tests were performed on a Teledyne-Taber Shear/Scratch Tester (Model 502). A conical diamond stylus with a 90 degree included angle and a spherical tip with a radius of 76 μm was used. With an adjustable weight, the applied normal load could be changed from 0 g to 1000 g. The scratching speed was constant over the load range and was measured to be about 1.8 mm/sec. All the tests were done at room temperature without lubrication on the surface.

2.3. Scanning electron microscopy

The topography of the scratched surface was studied by scanning electron microscopy. The surfaces were coated with a thin film of Au/Pd to prevent charging. The machine used was a Philips XFL-30 scanning

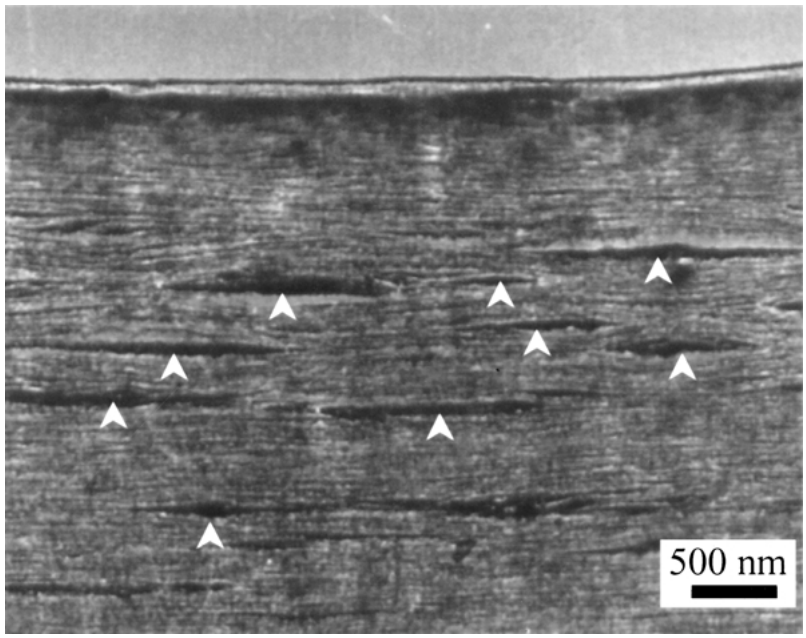

Figure 1 TEM image showing the near-surface morphology of rubber particles. The rubber particles were stained with RuO_4 and appeared gray in the TEM image, showing a well-elongated fibrous morphology. The talc particles appear black in the image and are marked with arrows.

electron microscope operated at an accelerating voltage of 5 kV.

2.4. Polarized optical microscopy

Semi-thin slices ($\sim$2 μm) of material around scratches were cut using a Reichert-Jung Ultracut-E microtome. Polarized light optical microscopy was conducted on a Nikon Optiphot optical microscope equipped with a Sony DXC-101 video camera. Images were digitized and stored on a Macintosh Power PC computer with a Scion Video Image 1000 8-bit frame grabber board. All the image analysis and measurements were done with the NIH Image program.

2.5. X-ray diffraction

The crystalline structure of the samples was studied by X-ray photography. Slices with thickness of $\sim$0.5 mm were cut from the different side-planes of the plaque with respect to the injection direction. The slice was then mounted on a 300 μm pinhole so that the point-collimated X-ray beam was focused on an area near the surface of the plaque. The X-ray diffraction patterns were obtained on a Rigaku Geigerflex generator with a fixed-tube copper K_α 0.1542 nm fine-focus X-ray source. Images were recorded on Kodak X-ray film and developed in Kodak GBX.

2.6. Transmission electron microscopy (TEM)

For the imaging of the scratched area, the sample was trimmed by cutting semi-thin ($\sim$2 μm thick) slices off until the area of interest was exposed. The trimmed blocks were then stained by ruthenium tetraoxide aqueous solution following standard procedures for about 1 hour [35]. A thin layer of gold was evaporated to mark the surface. The stained blocks were then embedded into low-viscosity epoxy resin before ultra-thin ($\sim$70 nm thick) slices were cut for the final TEM observation. Ultra microtomy was conducted on a Reichert-Jung Ultracut-E® with a Diatome® 45° diamond knife. TEM observation was performed on a JEOL 4000EX transmission electron microscope operated at 400 kV ($\lambda = 1.6$ pm). The unscratched surfaces were also imaged with TEM to study the morphology of rubber particles before scratching.

3. Results

3.1. Micro-morphology

Shown in Fig. 1 is the TEM image of the near-surface morphology of rubber particles taken from a cross-section parallel to the injection flow direction. Due to the staining of ruthenium tetraoxide, the rubber particles appear gray in this bright field image. As shown in the image, the rubber particles are highly elongated in the injection flow direction. X-ray diffraction taken from the near-surface area of the cross-section parallel to the injection-flow direction shows a typical fiber pattern, which indicates that the polypropylene polymer chains are also oriented in the injection flow direction (Fig. 2). To minimize the complication arising from the structural anisotropy on the deformation behavior, all the scratches discussed in the following text were obtained with the stylus dragging parallel to the injection flow direction.

3.2. SEM and polarized OM

SEM imaging of the scratched surface shows periodic deformation ridges arising from the plastic plowing of the tip over the surface (Fig. 3). No obvious change

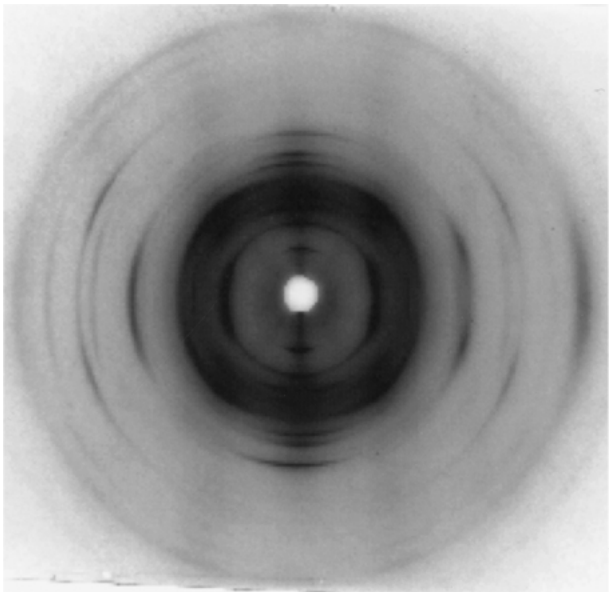

Figure 2 Wide angle X-ray diffraction pattern from near-surface area of parallel cross-section. The free surface of the sample was oriented horizontally.

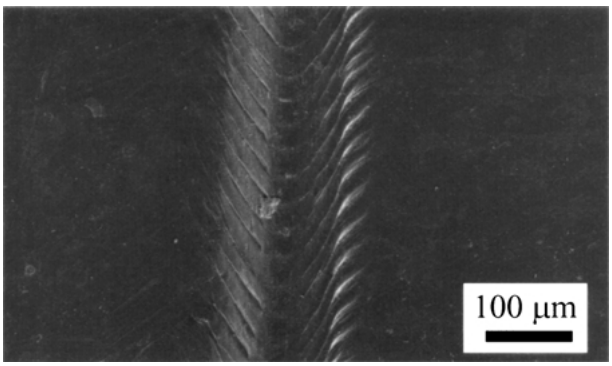

Figure 3 SEM image shows the top view of a 100 g load parallel scratch. The direction of the scratch is from top to bottom.

in the scratching pattern was observed in the range of applied normal load (0–1000 gms).

Shown in Fig. 4 is a polarized light optical microscop image of the strain field around an 800 g parallel scratch. Calibration with cold-drawn polypropylene fibers showed that the polymer chains are oriented parallel to the free surface around the scratch. Shown in Fig. 5 is a polarized light optical micrograph taken on the semi-thin slice cut from beneath the center of a 100 g scratch. A birefringent shear band structure can clearly be seen due to the localization of the plastic deformation, which causes different orientation of polymer chains inside and outside the deformation zone.

3.3. TEM observation

Shown in Fig. 6 is an ultra-thin (∼70 nm) TEM sample on a 200 mesh copper grid. This shows little wrinkling in the slice from sample preparation procedure. The distance between deformation ridges is about 30 μm for a 100 g parallel scratch, which is consistent with the SEM observation.

Fig. 7 shows a TEM image of the deformation underneath the center of a 100 g parallel scratch. The deformation ridges can be clearly seen and the separation distance is again consistent with the SEM observation. What is of strong interest is the shear-band structure revealed by this image. Most of the shear bands initiate from the front of the deformation ridge and propagate into the bulk of material at a characteristic tilting angle with respect to the original rubber orientation. As the distance from the free surface increases, the shear band's width decreases and the primary shear band splits into finer ones deep into the bulk. Some diffuse shear bands were also observed. No obvious voiding under the 100 g parallel scratch was observed. It was also interesting to notice that the talc particles bend at the shear band boundary, and there is no obvious evidence showing any influence of talc particles on the formation and evolution of shear bands. As for the behavior of talc particles in the near-surface deformation of TPO materials, more detailed discussions will be presented in another paper.

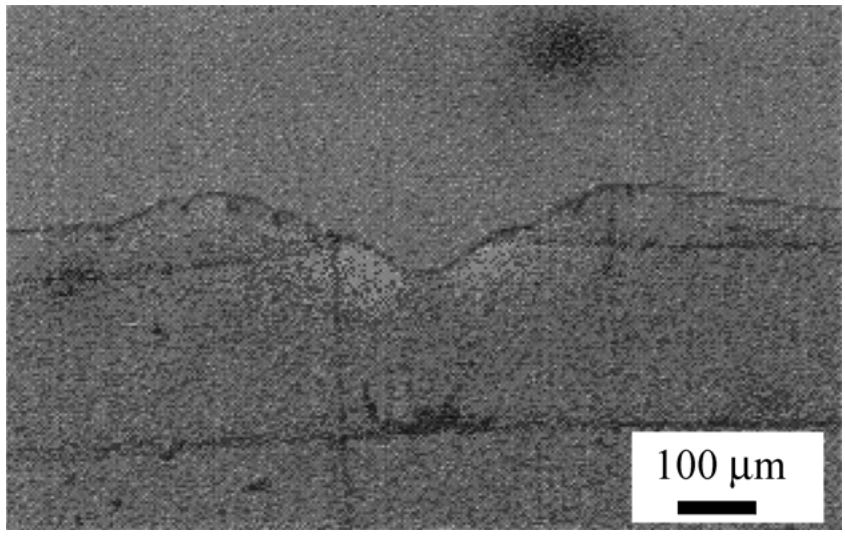

Figure 4 Polarized optical microscope image shows the birefringence around a scratch arising from the plastic deformation. The view direction is down the scratch direction.

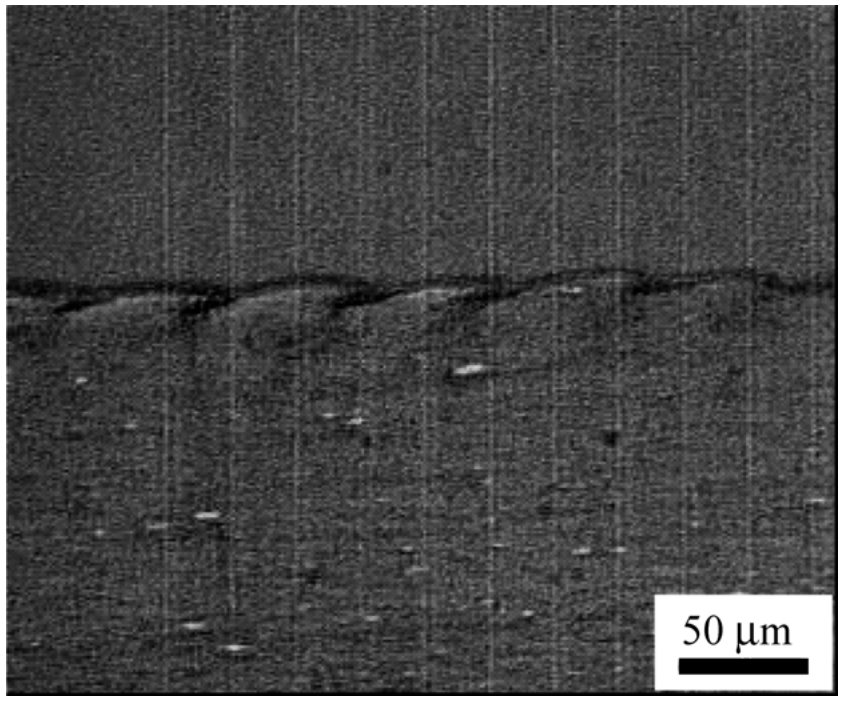

Figure 5 Birefringence from a semi-thin (∼2 μm) slice of material under the center of a 100 g scratch with the view plane parallel to the scratching direction. The direction of the scratch is from left of right.

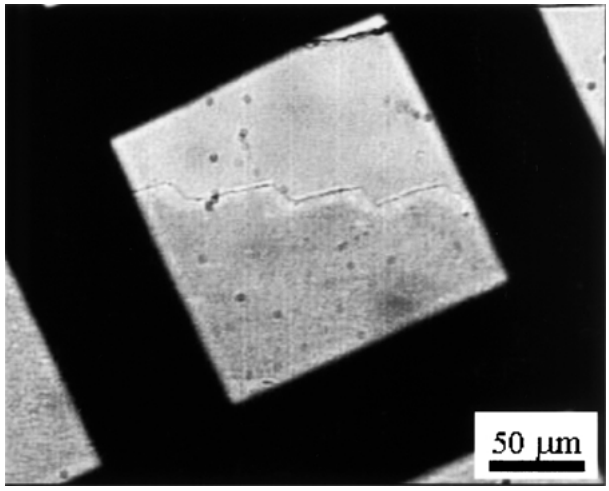

Figure 6 Optical microscope image of an utrathin (∼70 nm) slice of materials right underneath the center of a 100 g scratch mounted on a TEM copper grid. The direction of the scratch is from left to right.

4. Discussions

4.1. Microstructure of injection-molded polypropylene blends

Numerous papers have been published on the morphology and mechanical properties of PP/rubber blends [36 and references therein]. For injection molded polypropylene/EPDM rubber blends, Karger-Kocsis *et al*. [37] reported that there was a skin-core distribution of rubber particle morphology, i.e., near-surface rubber particles were well elongated and slim, while in bulk, they were large and less elongated. It was also observed that near the surface there was a thin PP-rich layer essentially without rubber particles. In the samples we studied, both a skin-core morphology and a thin PP-rich surface layer were observed. The thickness of thin PP-rich surface layer ranged from 0.5 μm to 3 μm. Several papers have been published on the PP-rich surface layer and apparently, the features of this layer depend on the specific processing and composition conditions [38, 39]. Because of the relatively large loads (>50 g) and penetration depth of the tip (∼150 μm for a 100 g parallel scratch) in our tests, this thin layer was not of significant concern in our scratching tests.

4.2. Deformation mode of materials

Fig. 8 shows the morphology of rubber particles around the boundary of a shear band. The rubber particles run continuously across the boundary. One conspicuous feature is that the rubber particles inside the shear band dilate as reflected by the larger width of the individual particles. Local Fast Fourier Transforms (FFT) of the image in areas inside and outside the shear band show different features in reciprocal space (Fig. 9). In the near surface area, the FFT image of the area outside the shear band shows a sharp streak, indicating a sharp boundary between the rubber particles and the matrix. The length of the streak is related to the average inter-particle distance. However, the streak in the FFT image inside the shear band is much shorter, which is consistent with a much larger average inter-particle distance due to material dilation in real space. The difference in the length of the streaks decreases with the increase in the distance from the free surface (Fig. 9). This change suggests that the extent of dilation decreases with the distance from the free surface. From a geometric analysis (Fig. 10), it is evident that the angles between the shear band boundary and rubber particles inside and outside the shear band give a measure of the dilation of material inside the shear band. The ratio between the

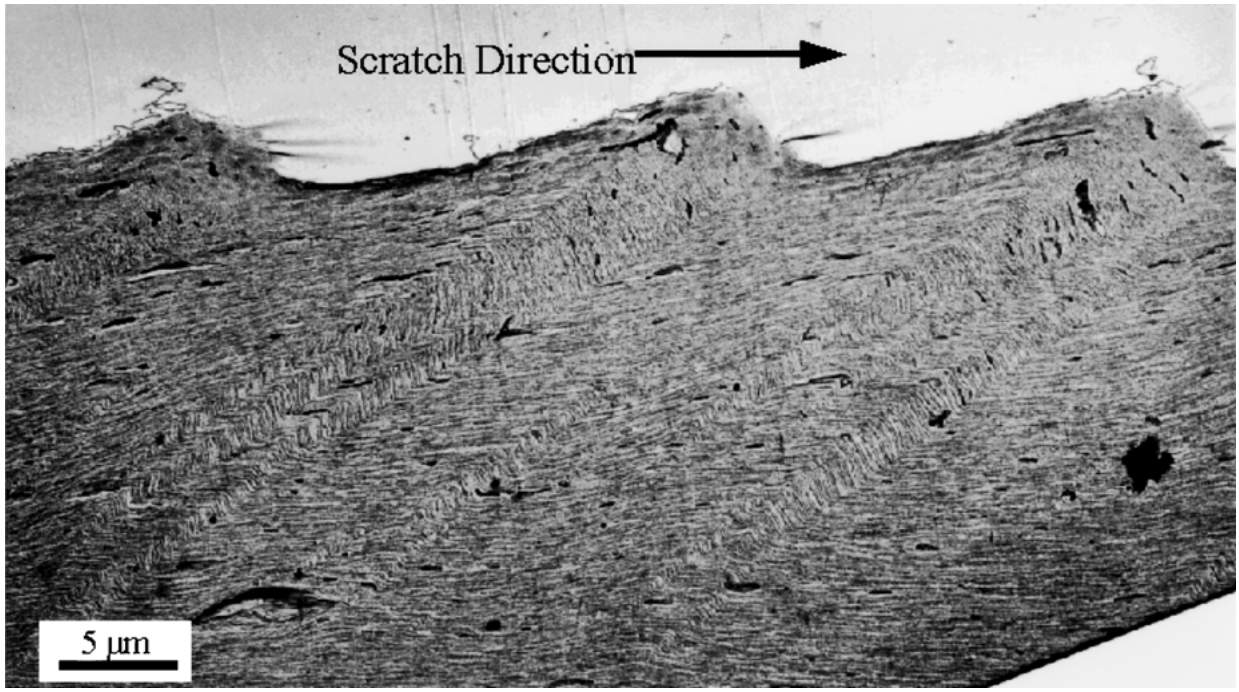

Figure 7 TEM image of deformation under the middle of a 100 g parallel scratch.

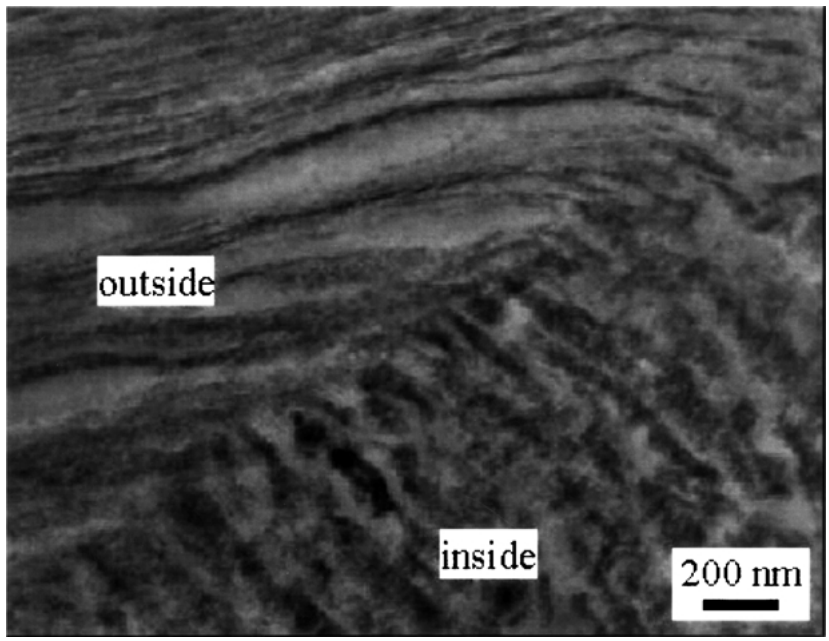

Figure 8 TEM image shows that rubber particles dilate inside shear bands.

sine values of these two angles equals the ratio of the corresponding inter-particle distances. We define here the extent of dilation E_d as the ratios between the sine values of the two angles:

$$E_d = \sin(\beta)/\sin(\alpha) \quad (1)$$

where β is the angle between the shear band boundary and rubber particles inside the shear band and α the angle between the shear band boundary and rubber particles outside the shear band. Fig. 11 shows that the angle β is always larger than α and decreases with the distance from the surface, while the angle α increases with the distance from the free surface. Shown in Fig. 12 is the calculated E_d at different distances from the free surface. The extent of dilation E_d monotonically decreases with increasing distance from the free surface, which is consistent with the results obtained from local FFT.

A number of papers have been published in recent years on the deformation mechanisms of PP-rubber blends [40–43]. Rubber particle cavitation [40] or crazing [41] was generally observed in the deformed material, which gave rise to voids with size from several hundred nanometers to several microns. In rubber toughened polymer blends, it has been widely accepted

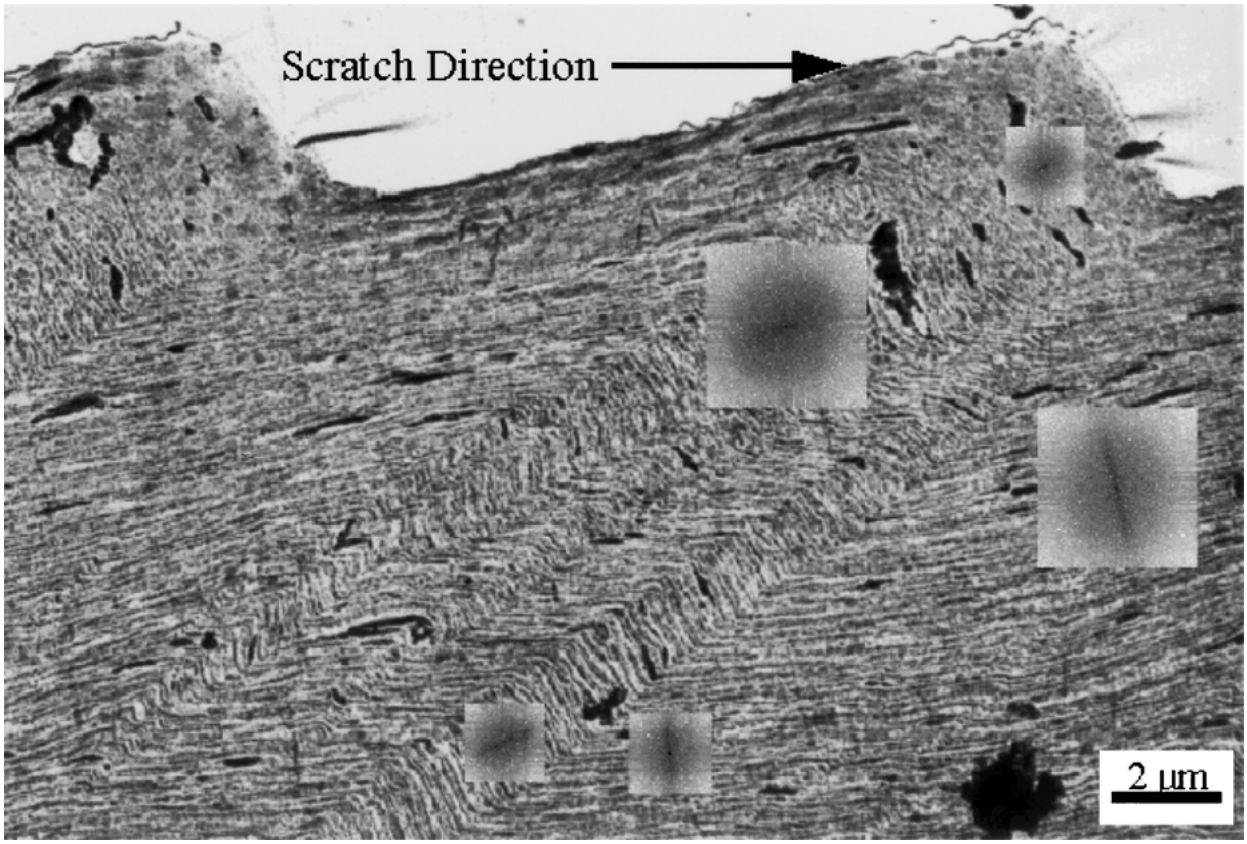

Figure 9 Fast Fourier transformation of areas inside and outside shear band in a TEM image.

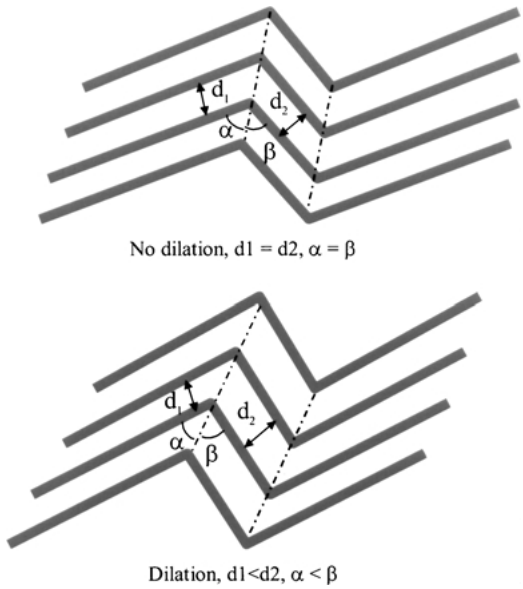

Figure 10 Correlation of the extent of materials dilation inside shear band with angles between shear band boundary and rubber particles.

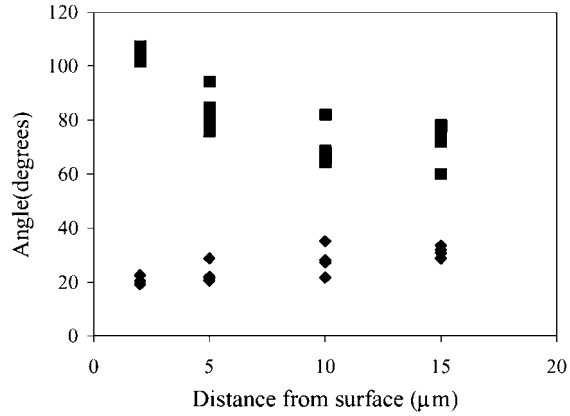

Figure 11 Change of angles with distance from free surface under a 100 g parallel scratch: between shear band boundary and rubber particles (♦) outside (α), and (■) inside (β) shear band.

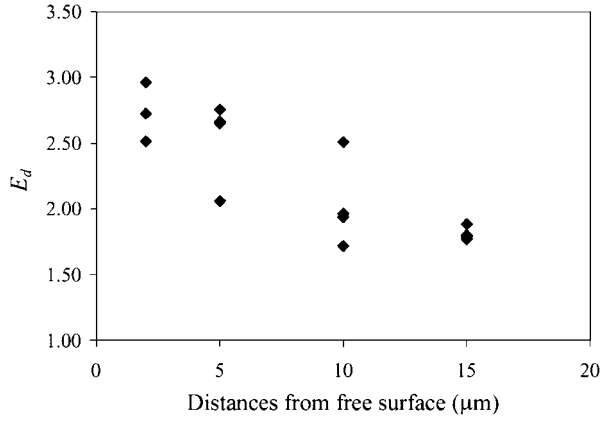

Figure 12 Extent of material dilation inside shear bands vs. distances from the free surface under a 100 g parallel scratch.

that rubber cavitation plays an important role in toughening by releasing bulk strain energy and triggering further shear deformation in the matrix [44].

Generally due to the relatively large bulk modulus, it is difficult to dilate before cavitation for rubber materials that have no defects other than inter-chain unoccupied volume [45, 46]. In our experiment, no obvious sign of voiding was observed inside the rubber particles. However, as shown in Fig. 13, we can clearly see crystalline lamella inside the rubber particles. Kausch *et al.* [47] have

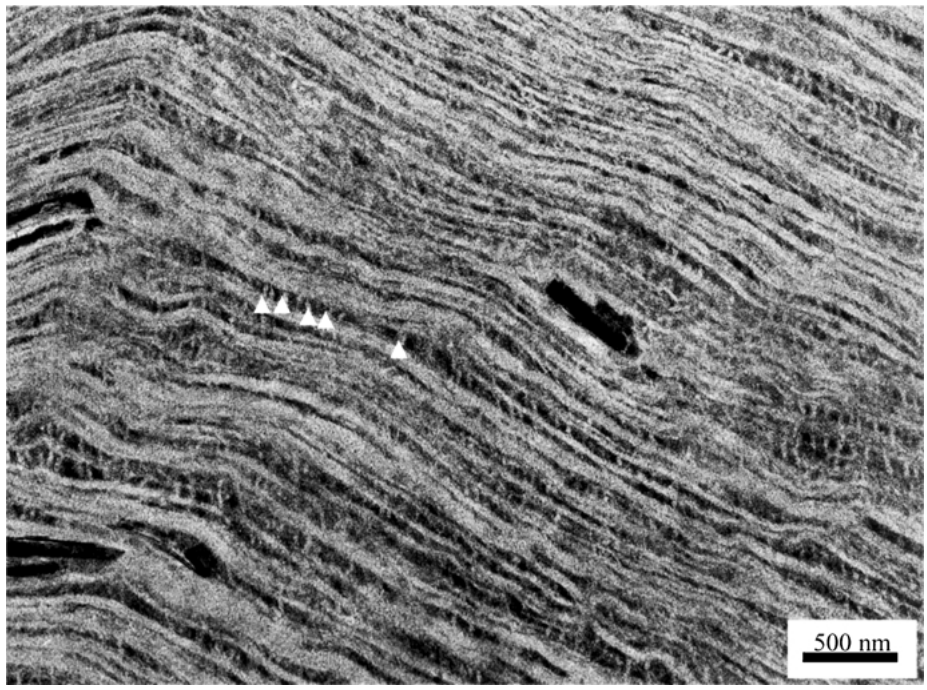

Figure 13 TEM image shows crystalline lamella inside rubber particles (some of them are pointed out by arrows).

pointed out that when deformed at temperature higher than T_g, local strain concentration due to the structural heterogeneities of the lamellar semicrytalline material will trigger a large amount of fine crazes. This makes us speculate that the observed dilation of materials inside the shear bands might be the relics of primitive crazing structures with voids of very small size (<70 nm, the estimated thickness of the TEM sample), which is beyond the resolution of this method due to the limit of sample thickness and the possible artifacts incurred during the process of staining and microtome. It is worth pointing out that generally shear deformation is considered a volume conservative process, which seems to contradict the material dilation we observed here. However due to the stick-slip motion between the scratching tip and the surface, the deformation of materials under scratching tip is not simply shearing. At the wake of the deformation ridge, materials undergo a tensile stress, which contributes to the dilation of materials inside the shear bands [1].

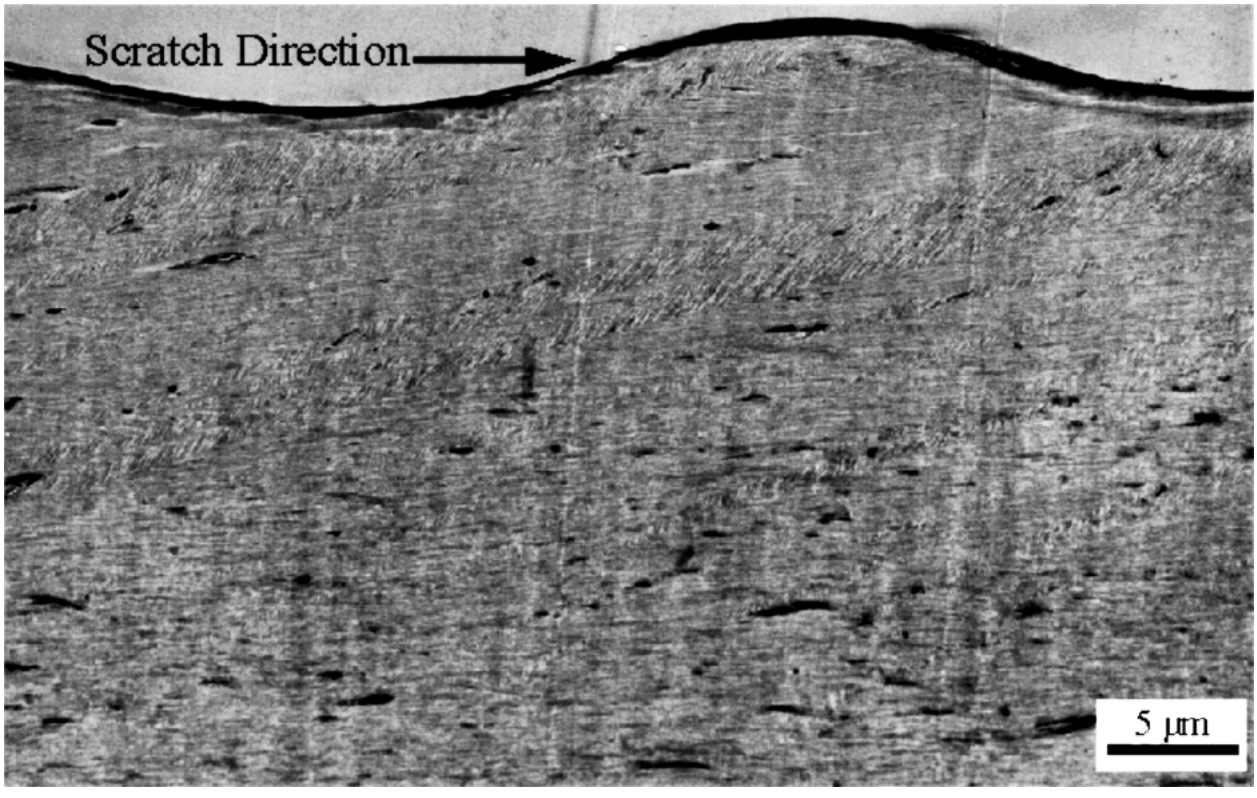

Figure 14 TEM image shows deformation under a 200 g parallel scratch.

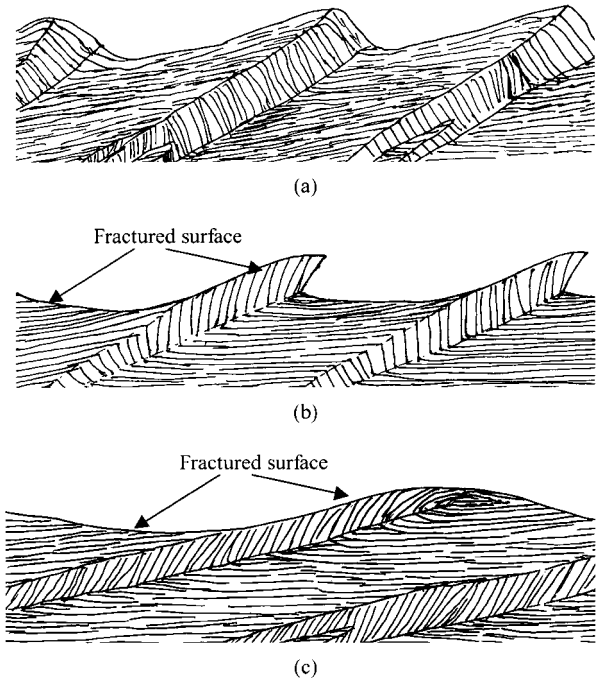

Figure 15 Schematics showing the sequence of the deformation mode under scratches in an injection-molded TPO plaque with increasing normal loads: (a) Step-like deformation ridge at low load, (b) initiative tearing and (c) tearing and ironing at high load.

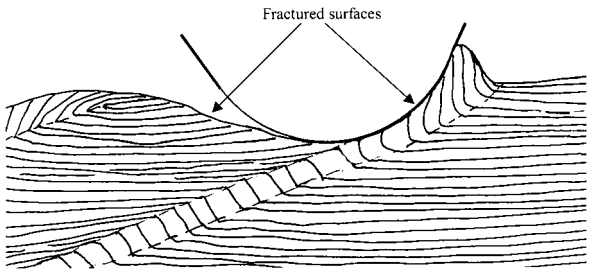

Figure 16 Schematic drawing of the material tearing by the sliding tip under a high applied normal load (>200 g).

4.3. Influence of applied normal loads on the deformation behavior

Shown in Fig. 14 is the deformation under a 200 g parallel scratch. The shape of the deformation ridge changes from a step-like shape at 100 g normal load to a lump-like shape at 200 g normal load. By following the traces of rubber particles, we can see that there is a possible fracture face, at which the rubber particles have been torn and fractured (Fig. 15b and c). A schematic drawing of the tearing of materials under the sliding tip is presented in Fig. 16. Due to the ironing effect of the tip, the surfaces where the fracture of materials happens are relatively smooth. At high load, the tearing of materials by the sliding tip might cause cracking at the valley of the deformation ridge due to the increasing tensile stress, as we can see in Fig. 17. It is possible to imagine that there might be a transitional stage at which the material tearing forms a tongue-shape as shown in Fig. 16b. In fact we did see this shape of the deformation ridge in 100 g scratch perpendicular to the injection flow direction [48]. This "ironing" effect of high normal load on the deformation ridge is also seen in SEM images (Fig. 18). It is clear from these images that the roughness near the center of the scratches decreases with increasing applied normal load. TEM imaging at higher magnification reveals that right underneath the deformation ridge, the material folds under the scratch tip and a local orientation defect was formed, which bears similarity with a +1/2 disclination defect that is usually seen in liquid crystalline materials (Fig. 19).

Shown in Fig. 20 is the change with the applied normal load of the angles formed by the shear band boundary with the rubber particles outside and inside the shear band at the same distance from the free surface. The calculated extent of the material dilation is shown in Fig. 21. The increase in the material dilation inside shear band with increasing applied normal load should contribute to the increasing light scattering of scratches with increasing loads.

At even higher applied normal loads (500 g, Fig. 22), a significant amount of voiding was observed under the surface scratch. Measurements of the scratch whitening from surface scratches in TPO materials conducted by Lau *et al*. [32] showed that the scratch whitening increased with the applied normal load and leveled off at high scratch load. Light scattering is mainly caused by the structural inhomogeneities arising from the

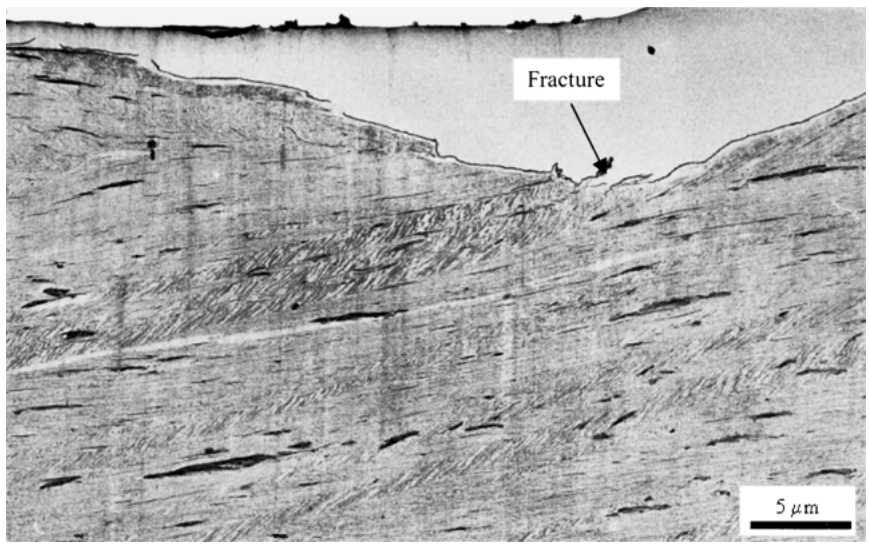

Figure 17 Fracture at a valley of the deformation waves under a 400 g parallel scratch.

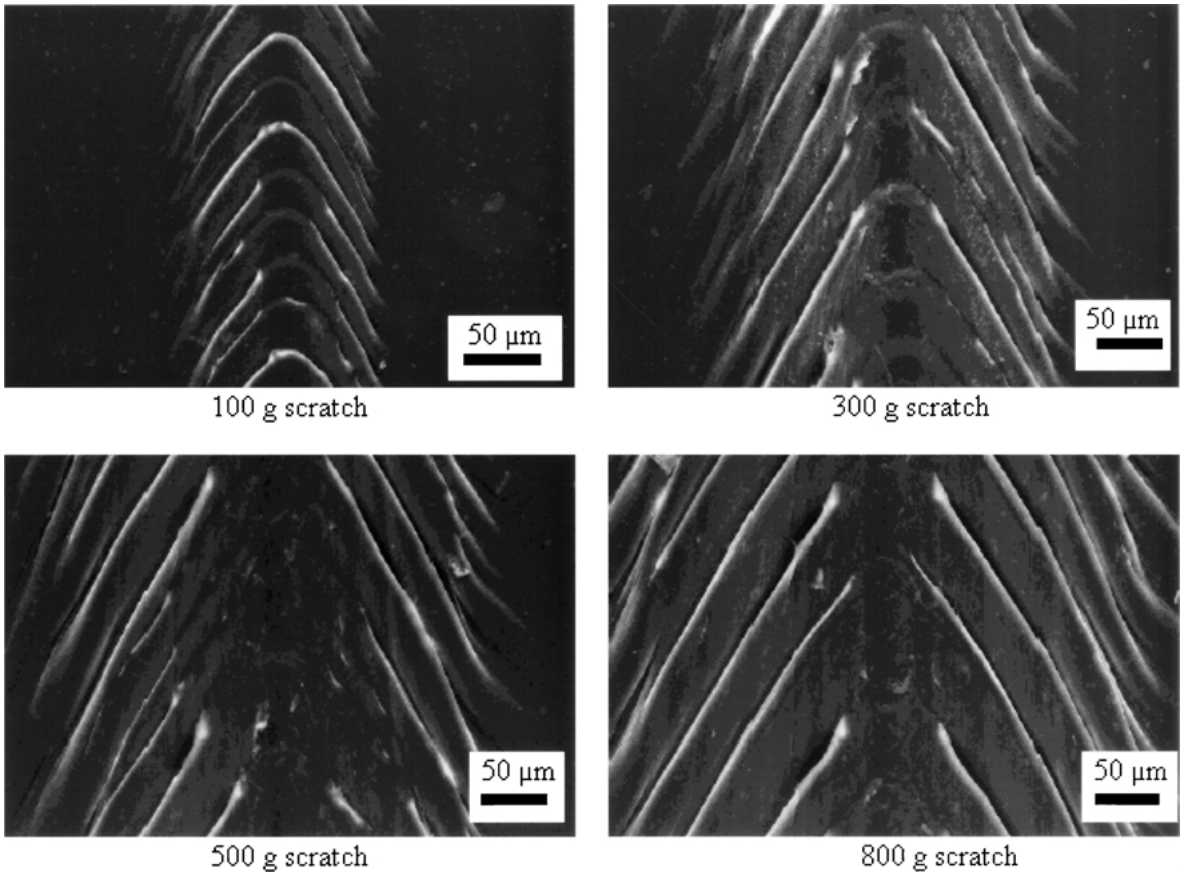

Figure 18 SEM images showing the ironing of deformation ridge near the center of the scratch notches at high load. The direction of scratch is from bottom to top.

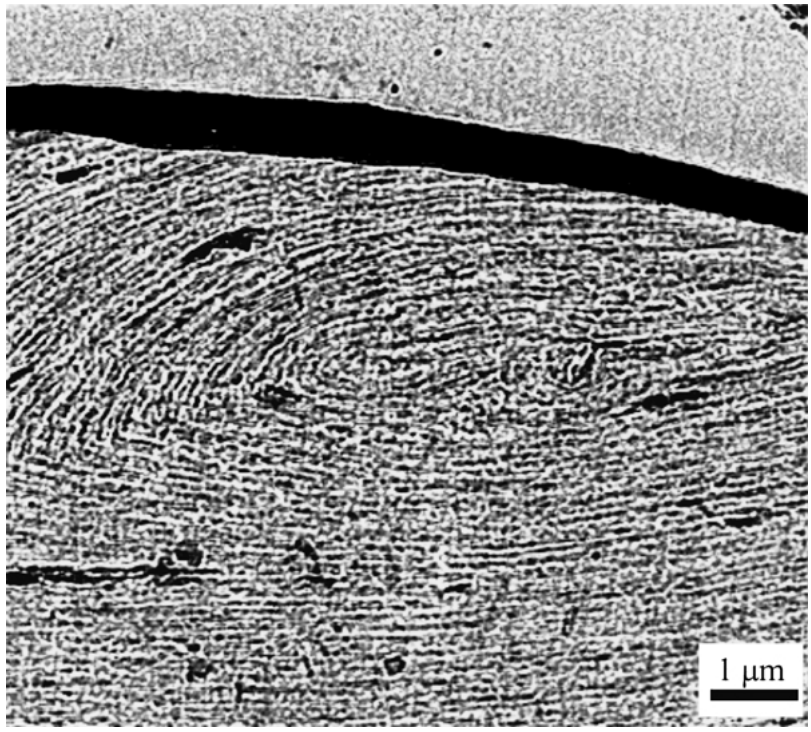

Figure 19 Local orientation defect right underneath the deformation ridge.

deformation of materials under scratches. The larger the applied normal load, the larger the volume of the materials deforms and thus the higher the intensity of the light scattering or scratch whitening. However when voiding happens, the air and the material interfaces play the dominant role in light scattering. Thus, the increase in the volume of deformed material with increased applied normal load no longer significantly

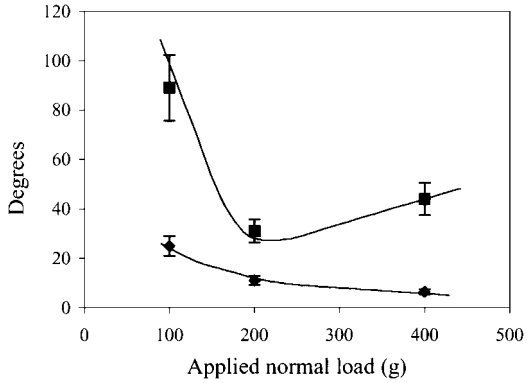

Figure 20 Change of angles with applied normal loads at a distance of 5 μm from the free surface: between shear band boundary and rubber particles outside (♦), and inside (■) shear band.

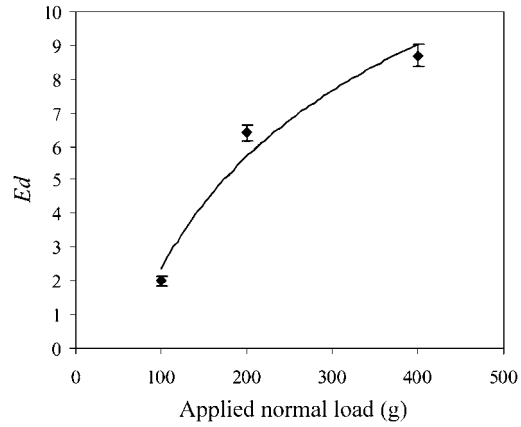

Figure 21 Change of the extent of material dilation (E_d) inside shear band with the applied normal load at a distance of 5 μm from the free surface.

influences the intensity of light scattering from the scratch. Another factor contributing to the light scattering is the surface roughness caused by scratches. As shown in Fig. 18, the roughness near the center of the scratch decreases with increasing applied normal load due to the ironing effect. Therefore, the surface roughness does not contribute significantly to the increase in scratch whitening with increasing normal load.

Our proposal that voiding is the dominant contribution to scratch whitening at high applied normal load was corroborated by the studies of stress whitening in impact modified PP. Rengarajan *et al*. [49] reported that when impact modifiers which promoted shear deformation were used, stress whitening in the toughened polypropylene was much less than in the blends in which impact modifiers triggered craze and void formation. Moreover, theoretical modeling showed that light scattering from voids is at least two orders of magnitude larger than that from rubber particles having a different density and refractive index from the matrix [50].

By checking Fig. 22, it can be seen that even though some cracks are around the talc particles, there is no obvious evidence showing a connection between the existence of talc particles and the crack initiation. Imaging at higher magnification showed that most of the cracks happened at the interfaces between the rubber particles and the PP matrix (Fig. 23). So a strong interfacial adhesion between the rubber particles and the matrix is desirable for improving scratch resistance by preventing the interfacial delamination between the rubber phase and the polypropylene matrix.

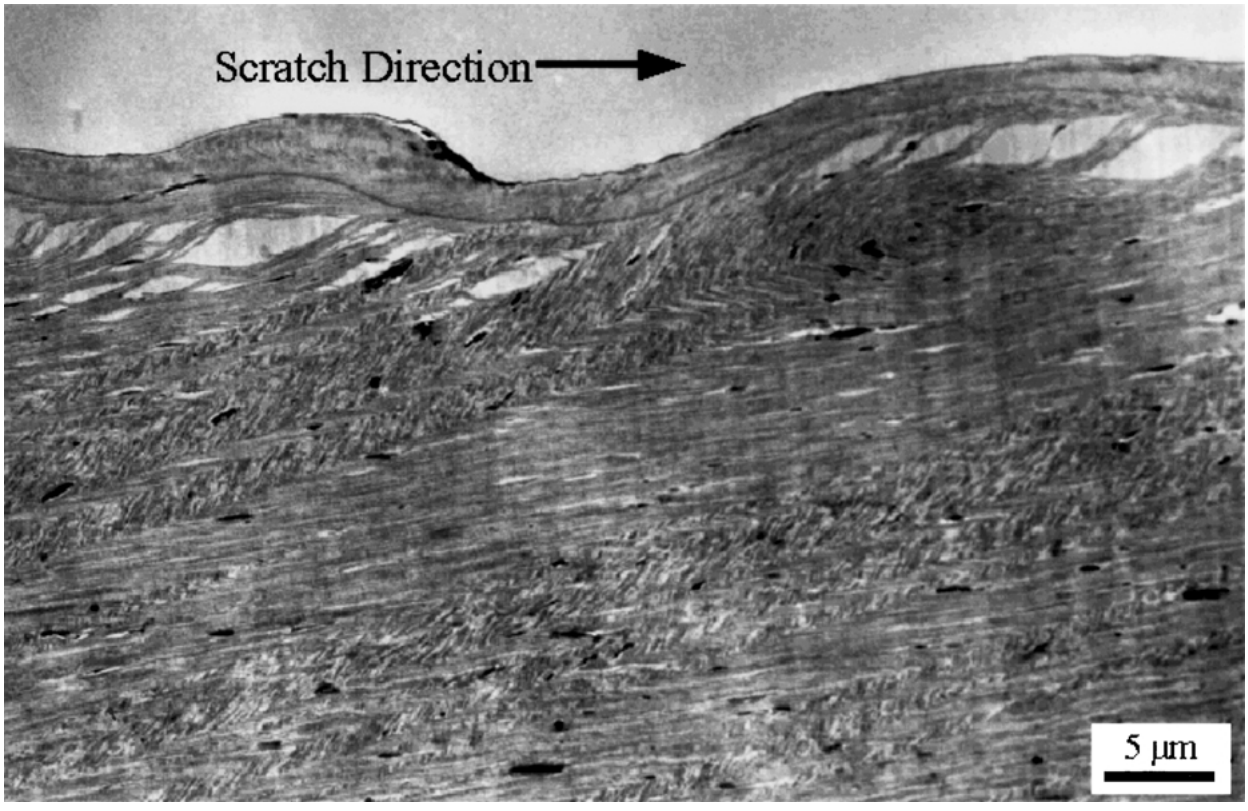

Figure 22 TEM image shows deformation under a 500 g parallel scratch.

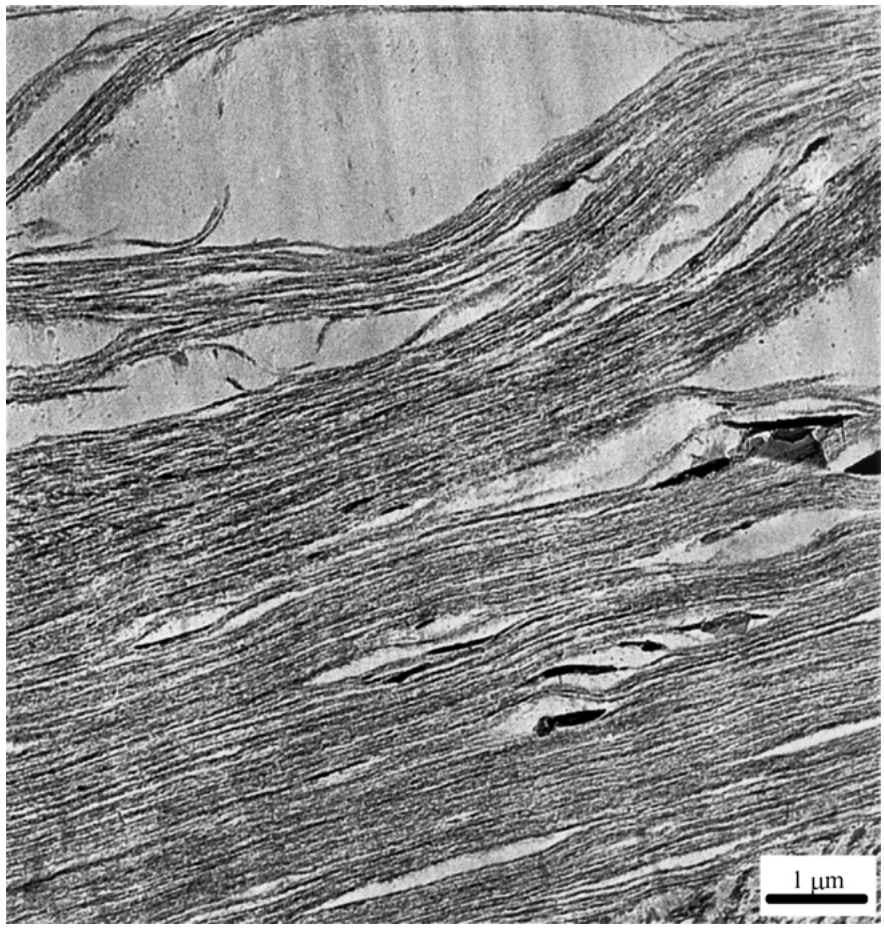

Figure 23 TEM image shows that under a 500 g scratch, voids nucleate through the debonding between rubber particles and the PP matrix.

5. Conclusions

We have characterized the near-surface plastic deformation under surface scratches in TPO materials with different microstructural characterization techniques. Our primary technique was TEM, which has the advantage of high spatial resolution and the ability to differentiate between phases after appropriate staining. The rubber particles near the surface area were highly oriented in the injection flow direction. It was observed that materials under surface scratches plastically deformed by forming periodic shear band structures. The shear band initiates from the front of the deformation ridge and propagates to the bulk at characteristic tilting angle with respect to the original rubber particle orientation. Dilation of rubber particles was observed inside the shear band. The extent of material dilation inside shear bands decreases with the increasing distance from the free surface and increases with the increasing applied normal load. At high normal load (>400 g), debonding occurred between rubber particles and matrix. These observations help us to understand the scratch whitening phenomenon in these very important industrial materials. We believe that this kind of deformation behavior was related to the near-surface rubber particle morphology. From this point of view, scratching tests, with the highly localized stress field, coupled with detailed structure characterization provide a promising approach in characterizing structure-property relationships of materials.

Acknowledgements

This project was supported in part by the National Science Foundation, Du Pont Automotive and Visteon Co. We would like to thank Dr. Robert Matheson at Du Pont and Dr. Rose Ryntz at Visteon for supplying samples and many fruitful discussions. The valuable comments and suggestions from Professor Albert Yee at University of Michigan are acknowledged.

References

1. A. SCHALLAMACH, *Wear* **17** (1971) 301.
2. G. A. D. BRIGGS and B. J. BRISCOE, *ibid.* **35** (1975) 357.
3. A. D. ROBERTS and A.G. THOMAS, *ibid.* **33** (1975) 45.
4. Y. UCHIYAMA and Y. ISHINO, *ibid.* **158** (1992) 141.
5. Y. FUKAHORI and H. YAMAZAKI, *ibid.* **171** (1994) 195.
6. *Idem.*, *ibid.* **178** (1994) 109.
7. *Idem.*, *ibid.* **188** (1995) 19.
8. V. COVENEY and C. MENGER, *ibid.* **233–235** (1999) 702.
9. K. FRIEDRICH (ed.), "Friction and Wear of Polymer Composites" (Elsevier, New York, 1986).
10. K. FRIEDRICH, Z. LU and A. M. HAGER, *Wear* **190** (1995) 139.
11. H. CZICHOS, D. KLAFFKE, E. SANTNER and M. WOYDT, *ibid.* **190** (1995) 155.
12. S. W. ZHANG, *Tribology International* **31** (1998) 49.
13. B. J. BRISCOE, P. D. EVANS, E. PELILLO and S. K. SINHA, *Wear* **200** (1996) 137.
14. B. J. BRISCOE, E. PELILLO and S. K. SINHA, *Polymer Engineering and Science* **36** (1996) 2996.
15. B. J. BRISCOE, *Tribology International* **31** (1998) 121.
16. K. J. LI, B. Y. NI, J. C. M. LI, *Journal of Materials Research* **11** (1996) 1574.

17. R. R. MEEHAN, J. KUMAR, M. EARL, E. SVENSON and S. J. BURNS, *J. Mater. Sci. Lett.* **18** (1999) 93.
18. C. CAUTHIER and R. SCHIRRER, *J. Mater. Sci.* **35** (2000) 2121.
19. R. KANEKO and E. HAMADA, *Wear* **162–164** (1993) 370.
20. S. M. SETZ, R. S. DURAN, D. R. FAGERBURG and L. T. GERMINARIO, in *Mat. Res. Soc. Symp. Proc.*, Vol. 522 (Materials Research Society, 1998) p. 211.
21. B. D. BEAKE, G. J. LEGGETT and P. H. SHIPWAY, *Polymer* **42** (2001) 7025.
22. G. S. BLACKMAN, L. LIN and R. R. MATHESON, *ACS Polymer Preprints* **39**(2) (1998) 1218.
23. L. LIN, G. S. BLACKMAN and R. R. MATHESON, *Progress in Organic Coatings* **40** (2000) 85.
24. R. S. KODY and D. C. MARTIN, *Polymer Engineering and Science* **36** (1996) 298.
25. J. CHU, L. RUMAO and B. COLEMAN, *ibid.* **38** (1998) 1906.
26. C. XIANG, H. J. SUE, J. CHU and K. MASUDA, *ibid.* **41** (2001) 23.
27. J. CHU, C. XIANG, H. J. SUE, and H. R. DAMON, *ibid.* **40** (2000) 944.
28. L. LIN, G. S. BLACKMAN and R. R. MATHESON, *ACS Polymer Preprints* **39**(2) (1998) 1224.
29. C. XIANG, H. J. SUE, J. CHU and B. COLEMAN, *J. Polym. Sci: Part B: Polym. Phys.* **39** (2001) 47.
30. P. Z. WANG, I. M. HUTCHINGS, S. J. DUNCAN, L. JENKINS and E. WOO, in Proceedings of SPE Automotive TPO Global Conference, 2000, p. 107.
31. P. RANGARAJAN, K. HARDING and V. WATKINS, *APS Bulletin* **46** (2001) 157.
32. E. LAU, S. SRINIVASAN and E. SZCZEPANIAK, in Proceedings of SPE Automotive TPO Global Conference, 2000, p. 209.
33. J. CHAPPELLE, M. MASALOVIC, K. RYAN and K. MUSSER, in Proceedings of SPE Automotive TPO Global Conference, 2000, p. 287.
34. K. L. WALTON, M. K. LAUGHNER, J. D. POMIJE and E. S. GISLER, in Proceedings of SPE Automotive TPO Global Conference, 2000, p. 195.
35. D. MONTEZINOS, B. G. WELLS and J. L. BURNS, *J. Polym. Sci.: Polym. Lett. Ed.* **23** (1985) 421.
36. J. KARGER-KOCSIS (ed.), "Polypropylene: Structure, Blends and Composites, Vol. 2: Copolymers and Blends" (Chapman & Hall, London, 1995).
37. J. KARGER-KOCSIS and I. CSIKAI, *Polym. Eng. Sci.* **27** (1987) 241.
38. J. H. SOUTHERN and R. L. BALLMAN, *J. Appl. Polym. Sci.* **24** (1979), 693.
39. F. M. MIRABELLA, N. DIOH and C. G. ZIMBA, in Proceedings of SPE Automotive TPO Global Conference, 1999, p. 183.
40. P. R. HORNSBY and K. PREMPHET, *J. Mater. Sci.* **32** (1997) 4767.
41. A. VAN DER WAL and R. J. GAYMANS, *Polymer* **40** (1999) 6067.
42. W. JIANG, S. C. TJONG and R. K. Y. LI, *ibid.* **41** (2000) 3479.
43. R. GENSLER, C. J. G. PLUMMER, C. GREIN and H.-H. KAUSCH, *ibid* **41** (2000) 3809.
44. A. F. YEE and R. A. PEARSON, *J. Mater. Sci.* **21** (1986) 2462.
45. I. M. WARD, "Mechanical Properties of Solid Polymers," 2nd ed. (Wiley, New York, 1983) p. 361.
46. A. LAZZERI and C. B. BUCKNALL, *Polymer* **36** (1995) 2895.
47. H.-H. KAUSCH, R. GENSLER, CH. GREIN, C. J. G. PLUMMER and P. SCARAMUZZINO, *J. Macromol. Sci.-Phys.* B **38** (1999) 803.
48. H.-X. TANG and D. C. MARTIN, *J. Mater. Sci.*, in press.
49. R. RENGARAJAN, S. K. KESAVAN, K. L. FULLERTON and S. LEE, *J. Appl. Poly. Sci.* **45** (1992) 317.
50. J. HOLOUBEK and M. RAAB, *Collect. Czech. Chem. Commun.* **60** (1995) 1875.

Received 13 December 2001
and accepted 26 August 2002